

Supplementary Information

Elucidating DNA binding of dithienylethenes from molecular dynamics and dichroism

Mathieu Linares, Haofan Sun, Michal Biler, Joakim Andréasson, and Patrick Norman

1. DTE dynamics

We investigated movements of P-antiparallel DTE1 within 25 ns of MD simulation. The distribution of two dihedral angles, namely the C5-C4-C2-C3 (φ_1) and C4-C5-C6-C7 (φ_2), is mainly between 0 - 30° and 40 - 90°, respectively (Fig. S1) suggesting that there is only one population in angle, hence no switch from clockwise to anticlockwise DTE is observed. Similar behavior is observed for M-DTE1, and again no switch in helicity is observed as the distribution of φ_1 and φ_2 dihedral angles are mainly found from -30 to 0°, and from -90 to -40°, respectively (Fig. S2).

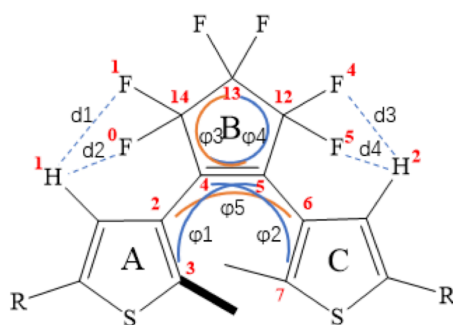


Illustration 1. Structure of DTE.

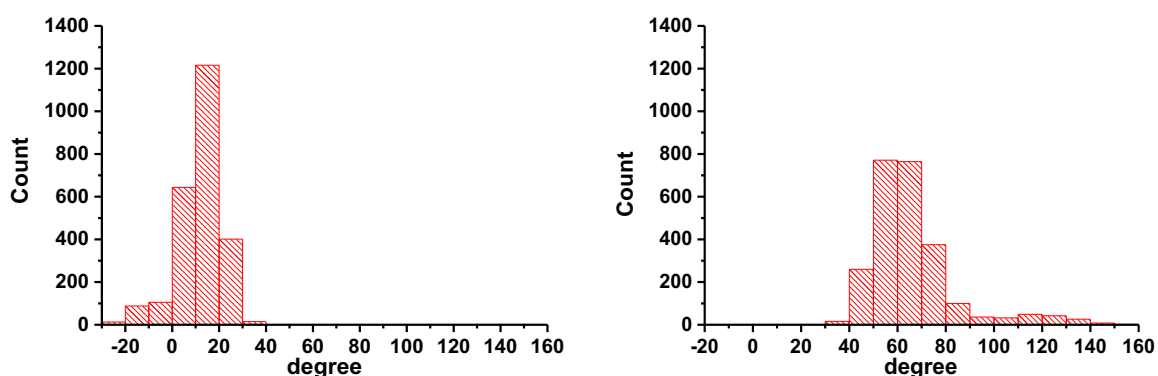


Figure S1. Population of the C5-C4-C2-C3 (φ_1 left) and C4-C5-C6-C7 (φ_2 right) dihedral angles of P-DTE1.

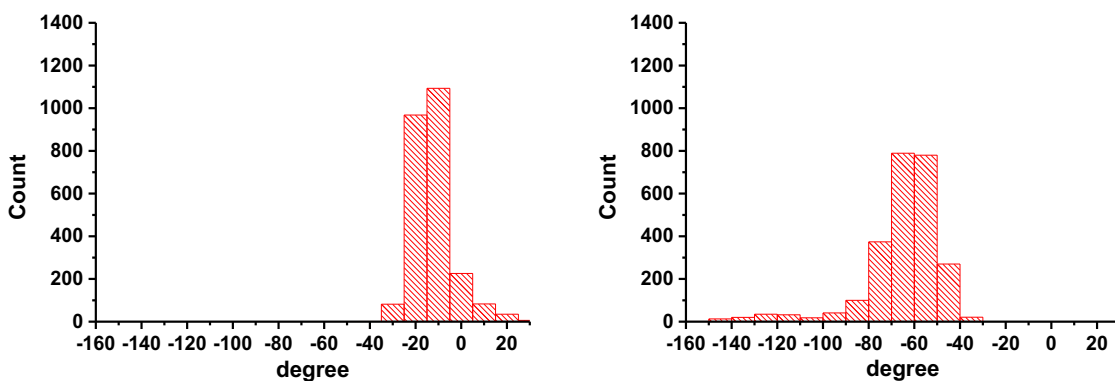


Figure S2. Population of the torsion angles ϕ_1 (left) and ϕ_2 (right) in M-DTE1.

These results indicate that DTE1 is not able to switch from P to M orientation within the MD timescale at 300 K. Hoping to fasten the switch from P to M orientation, we increased the temperature during the MD simulation to both 350 K and 400 K. Nevertheless, DTE is not able to change the helicity as the two dihedral angles were still around 0 - 30° (ϕ_1) and 40 - 80° (ϕ_2), and -15 - 25° (ϕ_1) and 20 - 80° (ϕ_2) for 350 and 400 K, respectively (Fig. S3, S4).

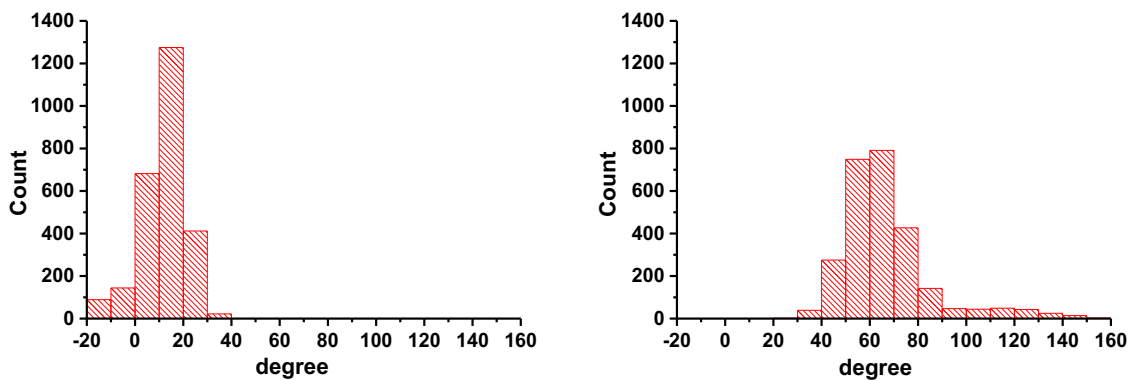


Figure S3. Population of the ϕ_1 (left) and ϕ_2 (right) dihedral angles of P-DTE1 within the MD timescale at 350 K.

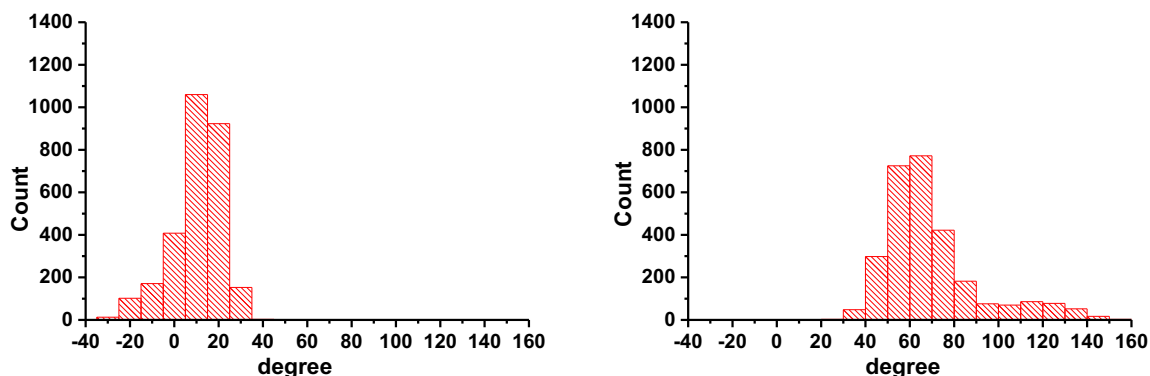


Figure S4. Population of the ϕ_1 (left) and ϕ_2 (right) dihedral angles of P-DTE1 within the MD timescale at 400 K.

The difference between these two angles, for both P-DTE1 and M-DTE1, is caused by the non-planar structure of the carbocycle B, where the dihedral angles within the cycle is not perfectly 0° (as seen in Fig. S5). This non-perfect planarity is a consequence of intramolecular H-bonding stabilizing interaction between either H1 or H2 and one of the fluorines. The distances distribution of H-bonds are shown in Fig. S6 and Fig. S7, summerized in Table S1. Hence, these distance differences make the carbocycle non-planar and also, this is the immediate cause of the difference between ϕ_1 and ϕ_2 .

The P-DTE2 and M-DTE2 behaves similarly as P/M-DTE1. The histograms of dihedral angles and H-bonds are shown in Figures S8-S11 and Table S1.

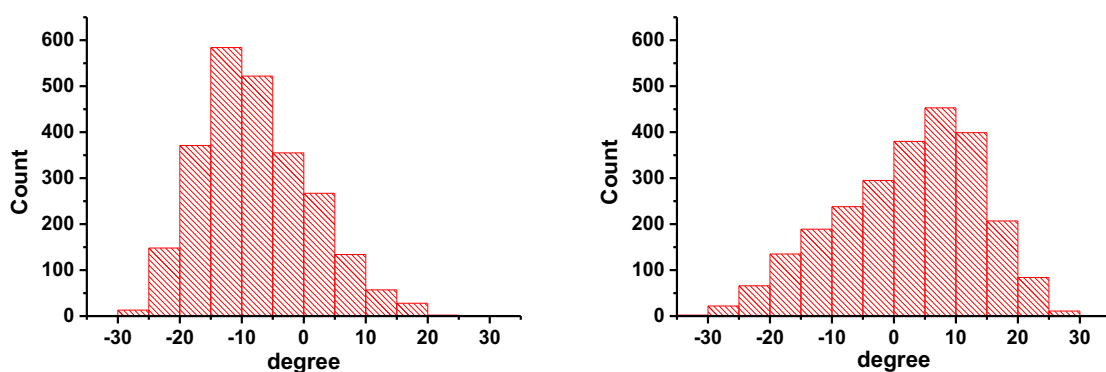
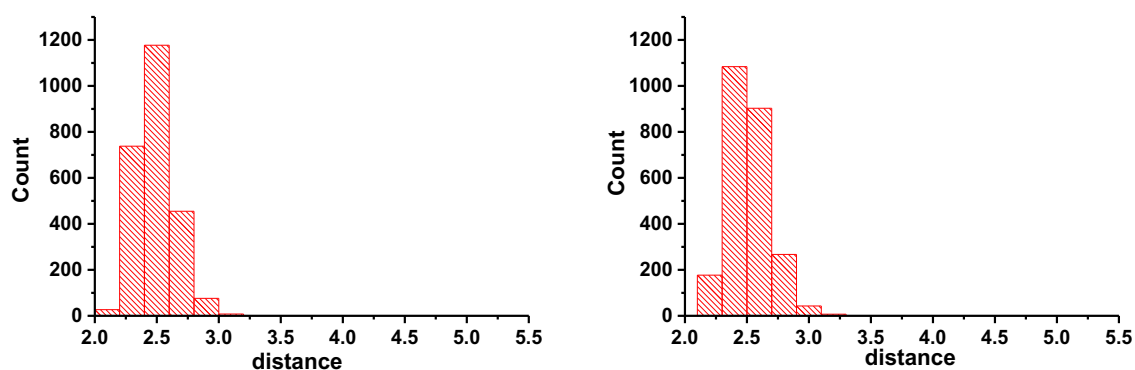


Figure S5. Population of the ϕ_3 (left) and ϕ_4 (right) dihedral angles within the B-ring of P-DTE1.



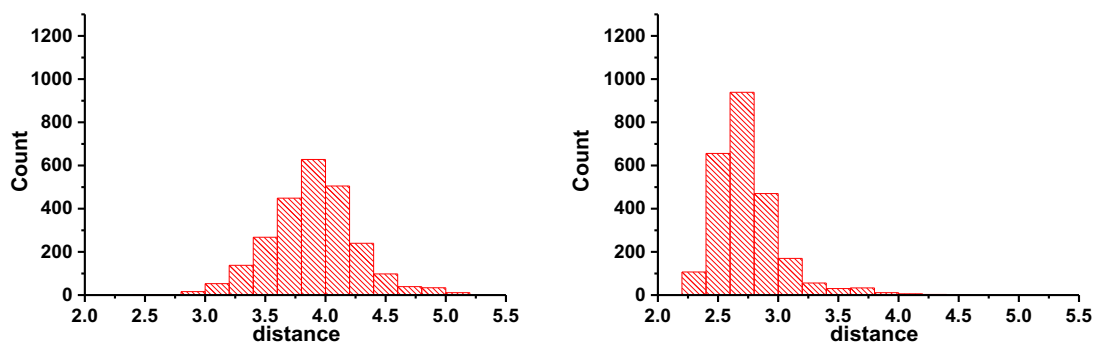


Figure S6. Population of the H-Bond distances between hydrogen and fluorine: H1-F1 (d1 upper left), H1-F0 (d2 upper right), H2-F4 (d3 bottom left) and H2-F5 (d4 bottom right).

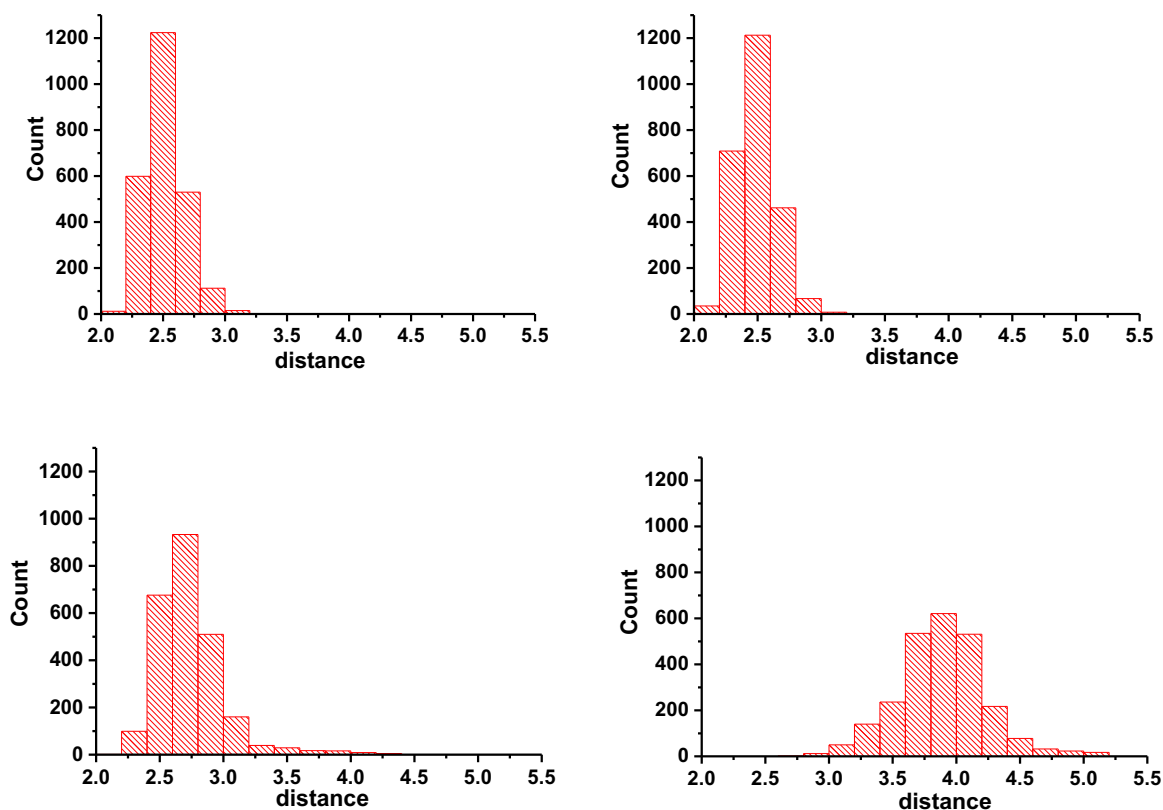


Figure S7. Population of the H-Bond distances between hydrogen and fluorine: d1 (upper left), d2 (upper right), d3 (bottom left) and d4 (bottom right) in M-DTE1.

Table S1. Population of the H-Bond distances mainly ranges between hydrogen and fluorine in different molecules.

	P-DTE1	M-DTE1	P-DTE2	M-DTE2
H1-F1 (d1)	2.2-2.8 Å	2.2-2.8 Å	2.2-2.8 Å	2.2-3.0 Å
H1-F0 (d2)	2.3-2.9 Å	2.2-2.8 Å	2.1-2.9 Å	2.2-2.8 Å
H2-F4 (d3)	3.2-4.6 Å	2.4-3.2 Å	3.2-4.6 Å	2.4-3.2 Å
H2-F5 (d4)	2.4-3.2 Å	3.2-4.6 Å	2.4-3.2 Å	3.2-4.4 Å

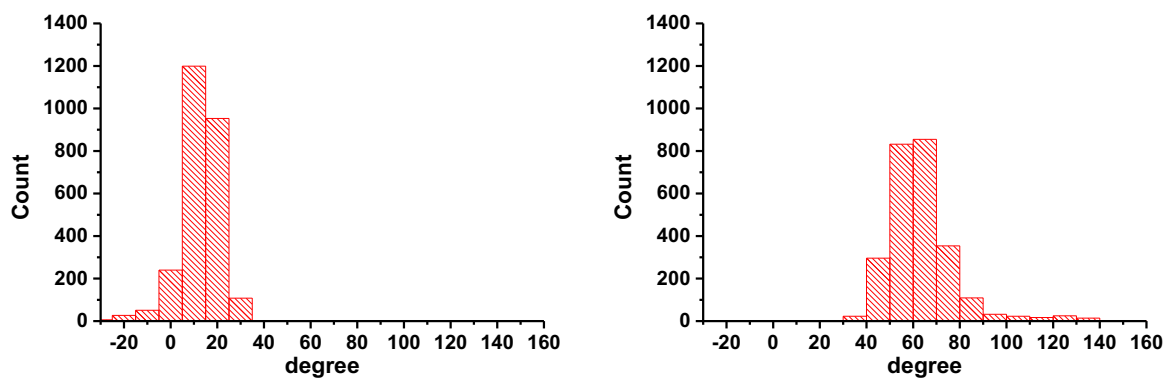


Figure S8. Population of the ϕ_1 (left) and ϕ_2 (right) dihedral angles of P-DTE2.

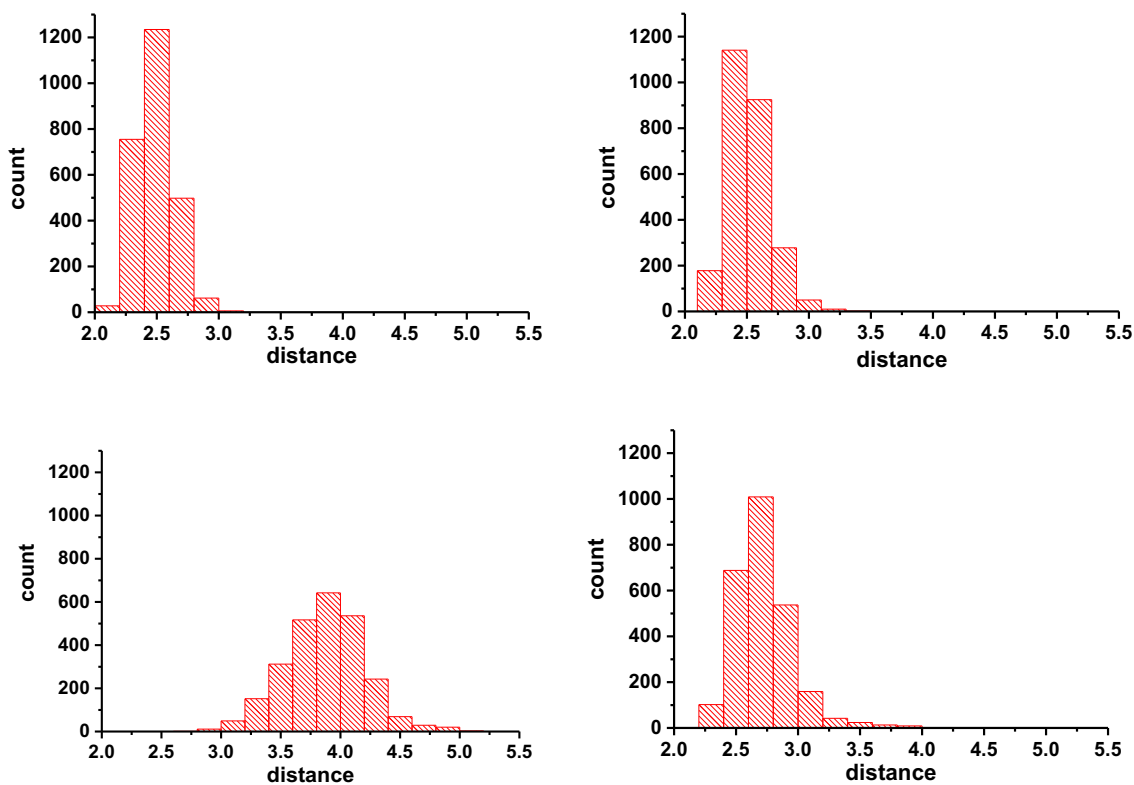


Figure S9. Population of the H-Bond distances between hydrogen and fluorine: d1 (upleft), d2 (upright), d3 (left bottom) and d4 (right bottom).

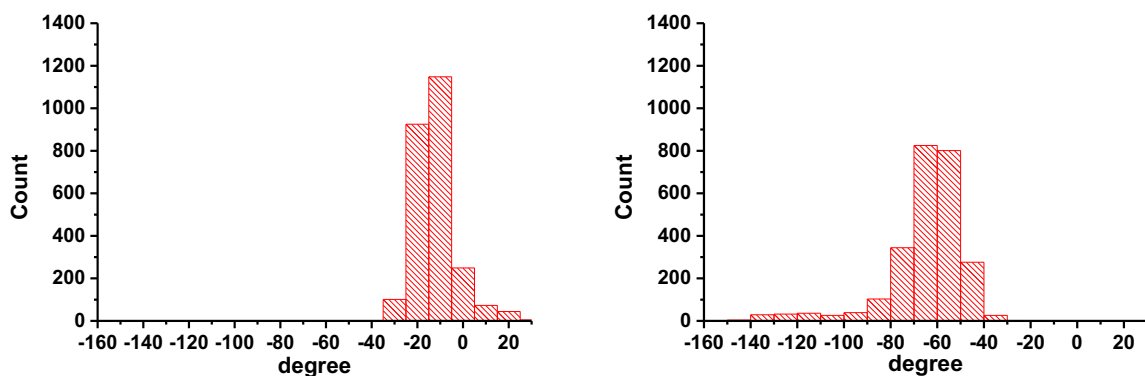


Figure S10. Population of ϕ_1 (left) and ϕ_2 (right) dihedral angles of the M-DTE2.

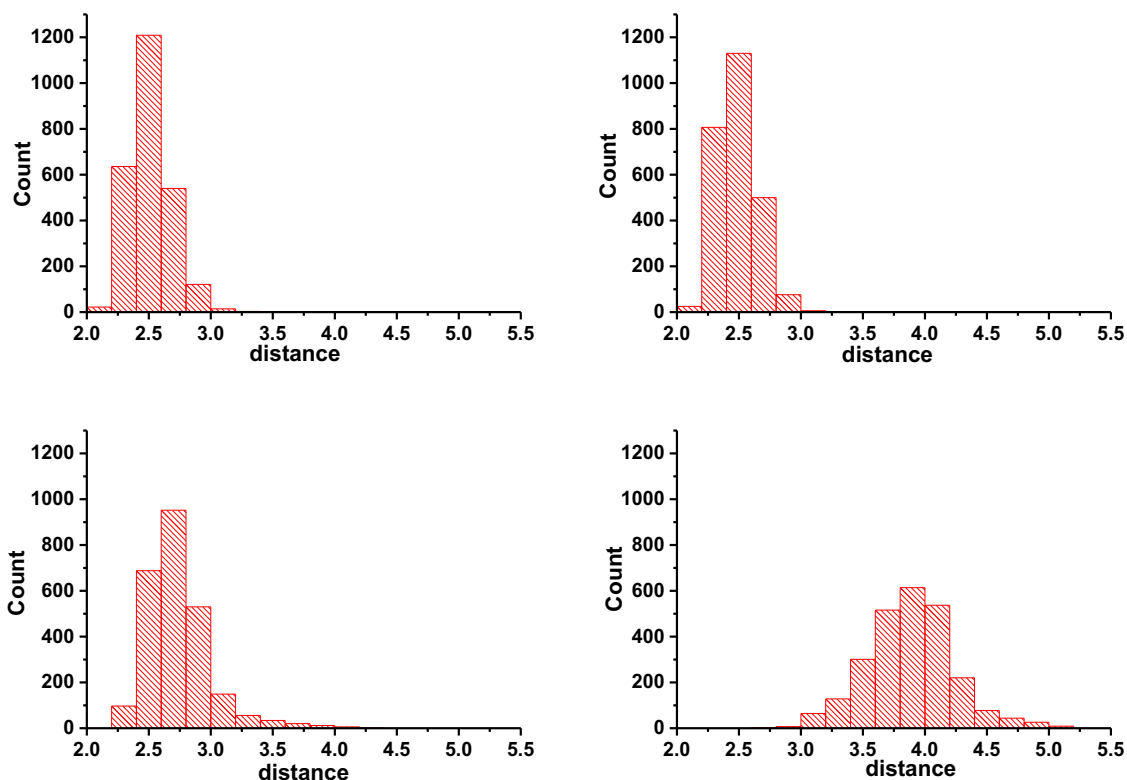


Figure S11. Population of the H-Bond distances between hydrogen and fluorine: d1 (upleft), d2 (upright), d3 (left bottom) and d4 (right bottom).

2. DNA–DTE interactions

First, we placed DTE in antiparallel conformer unbiasedly next to DNA. After the MD simulation, P-DTE1 approaches the major groove of DNA at around 4 ns and 12 ns but failed at binding to this place, and binds to the minor groove at around 18 ns (Fig. S12). The P-DTE2 binds directly to the minor groove (Fig. S13). M-DTE behaves similarly as P-DTE.

Then, we investigated DNA-DTE interaction biasedly for the four different binding poses.

For P-DTE1-antiparallel, the binding modes were as follow:

- 1) When the MD simulation started from the major groove binding pose, the interaction was not favorable as P-DTE1 escaped from the major groove (Fig. S14), not favorable position was also confirmed by high coulombic and vdW energies being -76 ± 26 and -17 ± 6 kcal/mol, respectively (Table S2). The molecule tried to bind to the minor groove afterwards, but it did not find a good favorable position to bind not even after 60 ns with the fluorine atoms pointing towards the base pairs. Then, the molecule moved to the bottom of 20 base pair long DNA, and it bound to the minor groove again, but at the same time it also bound to the bottom side of DNA. More precisely, the molecule bound to the minor groove with the

carbocycle C, whereas the other part of the molecule stayed at the bottom of DNA. This decreased the energies (Table 1) and stabilized the system.

- 2) When P-DTE1-antiparallel intercalated to DNA via the major groove, the molecule stayed in this binding pose during the whole MD simulation (Fig. S15). The base pair moved away from each other in order to create a space for the intercalation spot. Moreover, the molecule moved slightly deeper into DNA. The coulombic energy decreased from -130 ± 21 to -144 ± 19 kcal/mol, and the vdw energy decreased from -37.81 to -48.77 kcal/mol (Table S2 and Table 1) showing that the system is more stable and favorable than the binding mode no 1.
- 3) When the MD simulation started as the minor groove binding, the interaction between the DNA and P-DTE1 was not very favorable at first, and the carbocycle C moved away from the minor groove in order to turn itself into a more favorable position to bind to the minor groove, where it stayed bound the rest of the simulation (Fig. S16). This binding pose is mainly stabilized by coulombic interactions as the average coulombic energy is -190 ± 21 kcal/mol; the vdw energy increased about 6 kcal/mol (Table 1).
- 4) When the MD simulation started as an intercalation of P-DTE1-antiparallel via the minor groove (Fig. S17), the molecule stayed at the similar position for 29 ns with relatively high vdw energy (Table S2). Nevertheless later, the molecule moved towards the minor groove binding pose and stayed there until the end of the MD simulations (until 100 ns). Moreover, the base pairs, which moved away from each other when intercalation occurred in order to make a place for P-DTE1, returned to the expected position, where adenin and thymin forms hydrogen bonds. Since both poses no 3 and 4 ended up as minor groove binding, one would expect similitias in energies, which is not the case here (Table S2 and Table 1). In pose no 3, the molecule fully binds to the minor groove, hence it is more stabilized and the energy is lower, whereas in pose no 4, the molecule bound to DNA only by carbocycle C.

For P-DTE2, if we follow the same order of binding poses, the interactions are as follow:

- 1) The P-DTE2 does not stay in the major groove and moves away at around 16 ns (Fig. S18). Similarly to P-DTE1, it partly binds to the minor groove and it partly stays at the bottom of DNA. The coulombic and vdw energies decreased from the first 5 ns of MD simulation (Table S2) to the last 5 ns (Table 1), showing a stabilization effect, nevertheless the energies are still relatively high compared to other cases.


- 2) The P-DTE2 still stays in the major groove intercalation (Fig. S19). 
- 3) The molecule stays in the minor groove binding position (Fig. S20).
- 4) The molecule still stays in the minor groove intercalation (Fig. S21).

Table S2. Average (first 5 ns, 500 frames) coulombic and van der Waals energies for different binding positions between P-DTE1 or P-DTE2 and DNA.

	Initial binding position		Coulombic (kcal/mol)	vdW (kcal/mol)
P-DTE1	Major groove	Binding	-76±26	-17±6
		Intercalation	-130±21	-38±3
	Minor groove	Binding	-159±24	-41±6
		Intercalation	-124±12	-49±3
P-DTE2	Major groove	Binding	-97±31	-14±6
		Intercalation	-117±14	-45±4
	Minor groove	Binding	-211±14	-51±4
		Intercalation	-108±12	-46±3

Table S3. Average (first 5 ns, 500 frames) coulombic and van der Waals energies for different binding positions between M-DTE1 or M-DTE2 and DNA.

	Initial binding position		Coulombic (kcal/mol)	vdW (kcal/mol)
M-DTE1	Major groove	Binding	-69±27	-15±5
		Intercalation	-110±12	-44±4
	Minor groove	Binding	-196±15	-53±5
		Intercalation	-83±12	-42±3
M-DTE2	Major groove	Binding	-62±15	-19±5
		Intercalation	-115±9	-38±3
	Minor groove	Binding	-164±33	-38±5
		Intercalation	-86±13	-42±2

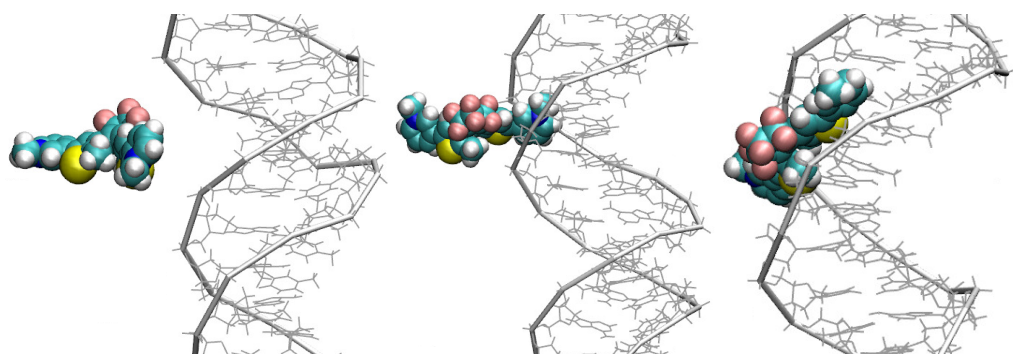


Figure S12. Unbiased docking for minor groove binding of P-DTE2.

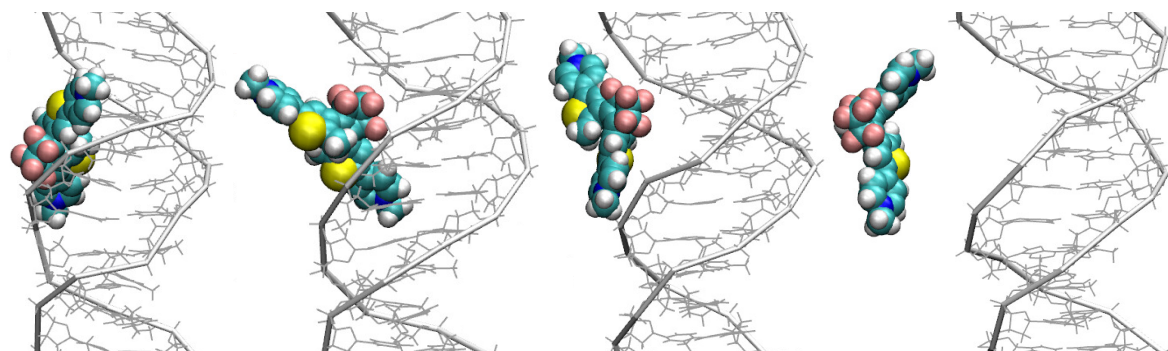


Figure S13. Escape from major groove binding of P-DTE1.

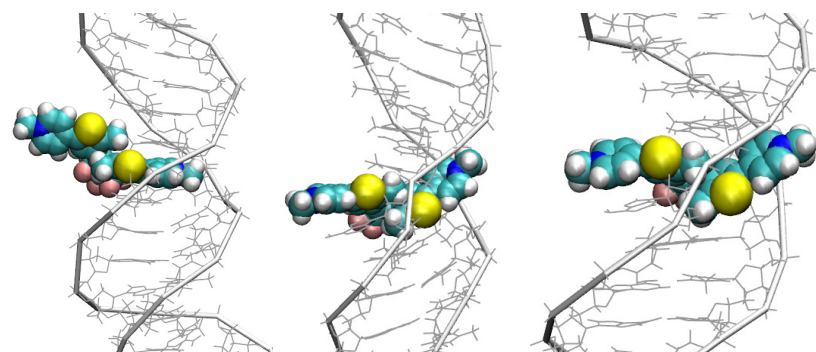


Figure S14. Evolution of major groove intercalation of P-DTE1.

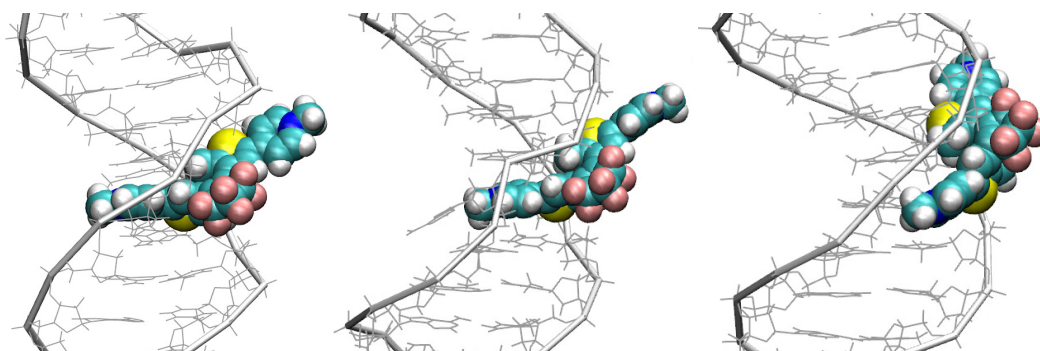


Figure S15. Escape from minor groove intercalation of P-DTE1.

Table S4. Averaged interaction energies (kcal/mol) for the last 5, 10, 20, and 30 ns for antiparallel methyl orientations in the open forms of DTE1 and DTE2.

		Major groove binding (MaGB)		Major groove intercalation (MaGI)		Minor groove binding (MiGB)		Minor groove intercalation (MiGI)		
		MD duration	Coulombic	vdW	Coulombic	vdW	Coulombic	vdW	Coulombic	vdW
DTE1	P	30 ns			-100±16	-31±5	-180±23	-41±6		
		20 ns			-104±16	-32±4	-179±22	-42±6		
		10 ns			-110±19	-34±5	-171±23	-43±6		
		5 ns			-115±25	-35±6	-170±26	-40±6		
	M	30 ns			-138±21	-48±5	-193±21	-41±5	-133±20	-53±5
		20 ns			-136±22	-48±5	-192±23	-41±5	-133±22	-52±5
		10 ns			-122±17	-45±5	-197±16	-42±4	-137±18	-52±4
		5 ns			-123±19	-43±5	-199±15	-43±3	-136±16	-51±4
DTE2	P	30 ns			-130±18	-50±3	-183±30	-47±7	-102±15	-48±4
		20 ns			-128±16	-49±3	-172±24	-45±7	-103±16	-48±4
		10 ns			-127±13	-49±3	-157±21	-41±6	-106±18	-48±4
		5 ns			-130±14	-49±3	-158±20	-44±4	-115±17	-49±4
	M	30 ns			-141±12	-53±3	-188±27	-39±6	-117±20	-51±4
		20 ns			-143±12	-53±3	-197±15	-41±3	-120±20	-51±4
		10 ns			-137±11	-52±3	-196±15	-41±3	-126±22	-52±4
		5 ns			-137±9	-53±3	-193±15	-41±3	-134±21	-53±3

Table S5. Averaged interaction energies (kcal/mol) for the last 5, 10, 20, and 30 ns for parallel and outside orientations of methyls in the open forms of DTE1 and DTE2.

		P-parallel		M-parallel		P-outside		M-outside		
		MD duration	Coulombic	vdW	Coulombic	vdW	Coulombic	vdW	Coulombic	vdW
DTE1	30 ns		-178±12	-55±4						
	20 ns		-177±13	-54±3						
	10 ns		-174±11	-53±4						
	5 ns		-176±11	-53±4						
DTE2	30 ns		-200±11	-55±3						
	20 ns		-201±11	-55±3						
	10 ns		-201±10	-56±3						
	5 ns		-201±10	-55±3						

Table S6. Averaged interaction energies (kcal/mol) for the last 5, 10, 20, and 30 ns for the closed forms of DTE1 and DTE2.

			Major groove binding (MaGB)		Major groove intercalation (MaGI)		Minor groove binding (MiGB)		Minor groove intercalation (MiGI)	
		MD duration	Coulombic	vdW	Coulombic	vdW	Coulombic	vdW	Coulombic	vdW
DTE1	P	30 ns	-52±33	-8±7	-117±9	-39±2	-177±16	-43±3	-114±17	-49±4
		20 ns	-61±32	-11±6	-118±9	-39±2	-177±16	-43±3	-116±16	-50±4
		10 ns	-68±23	-15±4	-121±8	-40±2	-180±15	-44±3	-118±17	-51±4
		5 ns	-71±21	-16±4	-117±9	-40±2	-181±15	-44±3	-121±15	-52±4
	M	30 ns			-166±17	-50±3	-198±17	-51±4	-145±19	-56±4
		20 ns			-165±17	-50±3	-193±16	-50±4	-147±16	-57±3
		10 ns			-164±15	-50±3	-193±17	-50±4	-142±17	-57±3
		5 ns			-166±15	-50±3	-190±16	-49±3	-147±14	-57±4
DTE2	P	30 ns			-116±8	-39±2	-228±19	-51±3		
		20 ns			-117±9	-39±3	-224±19	-51±4		
		10 ns			-114±9	-39±2	-217±12	-50±3		
		5 ns			-112±7	-39±2	-216±11	-49±3		
	M	30 ns			-113±9	-39±2	-207±13	-52±3		
		20 ns			-114±10	-39±2	-205±12	-51±3		
		10 ns			-113±7	-39±2	-207±12	-52±3		
		5 ns			-113±7	-39±2	-208±12	-52±3		

3. Circular Dichroism

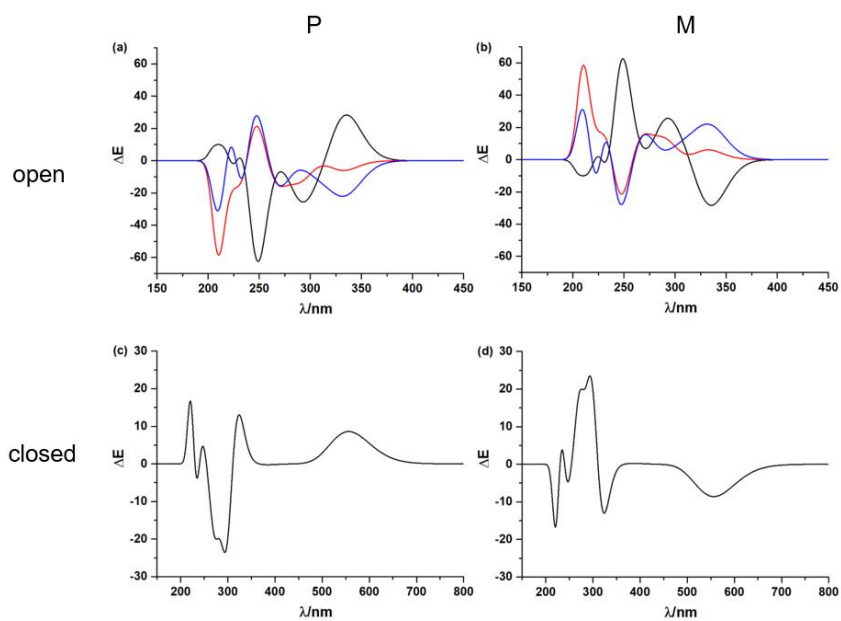


Figure S16. CD spectra for the open and closed forms of core DTE. Antiparallel conformation in black, parallel in red, and outside in blue. DFT/B3LYP optimized structures are adopted.

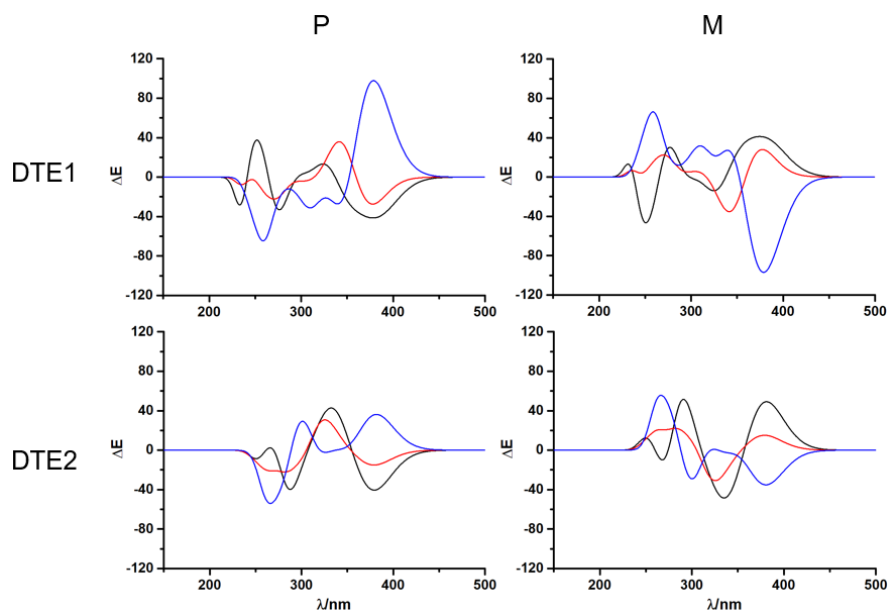


Figure S17. CD spectra for the open forms of DTE1 and DTE2. Antiparallel conformation in black, parallel in red, and outside in blue. DFT/B3LYP optimized structures are adopted.

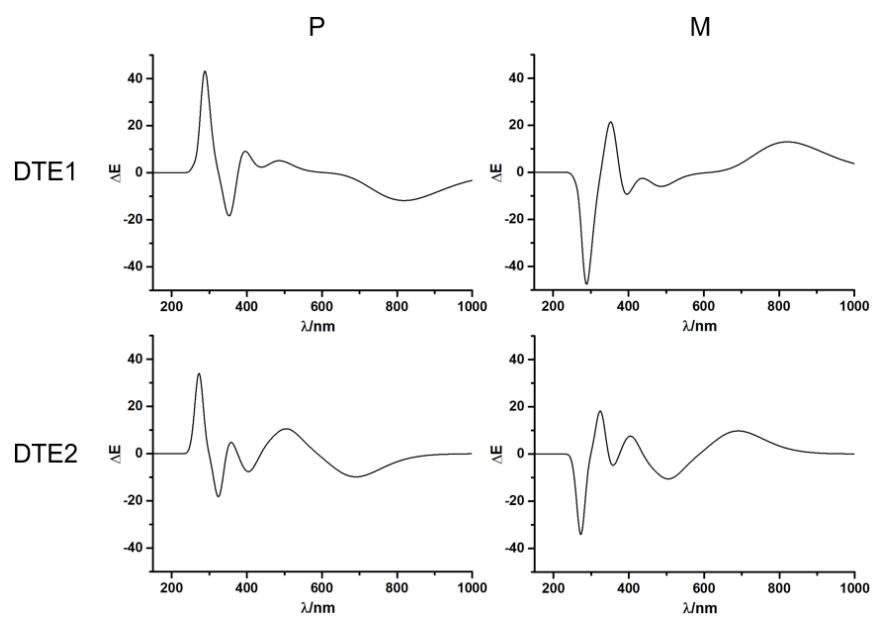


Figure S18. CD spectra for the closed forms of DTE1 and DTE2. DFT/B3LYP optimized structures are adopted.